Inverse Electrostatic Effect: Electrostatic Repulsion in the Unfolded State Stabilizes a Leucine Zipper[†,‡]

Daniel N. Marti* and Hans Rudolf Bosshard

Institute of Biochemistry, University of Zürich, Winterthurerstrasse 190, CH-8057 Zürich, Switzerland

Received June 14, 2004; Revised Manuscript Received July 23, 2004

ABSTRACT: The pH-dependent stability of a protein is strongly affected by electrostatic interactions between ionizable residues in the folded as well as unfolded state. Here we characterize the individual contributions of charged Glu and His residues to stability and determine the NMR structure of the designed, heterodimeric leucine zipper AB consisting of an acidic A chain and a basic B chain. Thermodynamic parameters are compared with those of the homologous leucine zipper AB_{SS} in which the A and B chains are disulfide-linked. NMR structures of AB based on ^{1}H NMR data collected at 600 MHz converge, and formation of the same six interchain salt bridges found previously in disulfide-linked AB_{SS} [Marti, D. N., and Bosshard, H. R. (2003) *J. Mol. Biol. 330*, 621−637] is indicated. While the structures of AB and AB_{SS} are very similar, their pH-dependent relative stabilities are strikingly different. The stability of AB peaks at pH ∼4.5 and is higher at pH 8 than at pH 2. In contrast, AB_{SS} is most stable at acidic pH where no interhelical salt bridges are formed. The different energetic contributions of charged Glu and His residues to stability of the two coiled coil structures were evaluated from pK_a shifts induced by folding. The six charged Glu residues involved in salt bridges stabilize leucine zipper AB by 4.5 kJ/mol yet destabilize disulfide-linked AB_{SS} by −1.1 kJ/mol. Two non-ion-paired Glu charges destabilize AB by only −1.8 kJ/mol but AB_{SS} by −5.6 kJ/mol. The higher relative stability of AB at neutral pH is not caused by more favorable electrostatic interactions in the folded leucine zipper. It is due mainly to unfavorable electrostatic interactions in the unfolded A and B chains and may therefore be called an *inverse electrostatic effect*. This study illustrates the importance of residual interactions in the unfolded state and how the energetics of the unfolded state affect the stability of the folded protein.

The free energy of unfolding of a protein is the difference between the free energies of the folded and unfolded states ($\Delta G_U = G_U - G_F$). G_U and G_F are the absolute free energies of the unfolded state and folded state, respectively, and ΔG_U is the free energy necessary to unfold the protein. When discussing the stability of a protein, one is tempted to consider only the folded state. Since there can be residual interactions in the unfolded state, a change in G_U may influence protein stability as well (*1*−*7*). However, it is difficult to assign a change in the stability of a protein to a a change in the stability of its unfolded state, which, for practical purposes, is an ensemble of states induced by chemical denaturants or heat.

Coiled coils are simple protein models that may be used to differentiate between effects of the folded and unfolded states on protein stability. The coiled coil structure is defined by an array of heptad repeats [$(abcdefg)_n$]. Heptad positions *a* and *d* are preferably occupied by hydrophobic residues, and the remaining positions often contain polar or ionizable residues. Three-dimensional structures of dimeric coiled coils, the so-called leucine zippers, have been determined by X-ray crystallographic or NMR methods (*8*−*12*). In the structures, two α-helices are wound around each other to form a superhelix. Hydrophobic residues in the *a* and *d* positions shape the hydrophobic interface of the coiled coil. In addition, ionizable residues in heptad positions *e* and *g* contribute to the integrity of the coiled coil in two ways. (i) By maintaining hydrophobic contacts between their methylene groups and *a* and *d* position residues of the chain interface, they strengthen the hydrophobic core and favorably contribute to stability (*8*, *11*, *12*). (ii) By being oriented toward each other, charged residues in positions[1] *g* and *e′*(+1) form attractive or repulsive electrostatic interactions between the component chains of the coiled coil. Indeed, repulsive interchain ionic interactions can prevent a leucine zipper from being formed (*13*−*18*). Stabilization of a leucine zipper by attractive interchain ion pairing, i.e., by interchain salt bridges, is less obvious (*12*, *19*−*22*). Double mutant thermodynamic cycles have been used to assess electrostatic interactions between the chains of a leucine zipper, and favorable coupling energies of 1.5−2.5 kJ/mol were reported (*23*−*25*). The coupling energy, however, mainly reflects the direct charge−charge interaction of the paired residues which is always favorable for opposite charges and does not disclose

[†] This research was supported in part by Grants 3100-055308 and 3100-100106 from the Swiss National Science Foundation.

[‡] The coordinates have been submitted to the Brookhaven Protein Data Bank (entry 1U2U).

* To whom correspondence should be addressed. Phone: +41 1 635 5545. Fax: +41 1 635 6805. E-mail: dmarti@access.unizh.ch.

[1] Positive and negative numbers in parentheses indicate up- and downstream shifts in heptads; dashes designate heptad positions of the adjacent helix.

10.1021/bi048771t CCC: $27.50
Published on Web 09/11/2004

the net energetic contribution to the stability of the salt bridge (*22*, *26*).

Alternatively, electrostatic interactions can be quantified by comparing the pK_a values of ionizable residues in the folded and unfolded protein (*26*). An upshifted pK_a value of a Glu side chain or a downshifted pK_a value of a His side chain is direct thermodynamic proof that the charged side chain destabilizes the folded protein (*19*, *26*, *27*). As with double mutant cycles, shifts of pK_a values do not report the entire energetic balance of salt bridges. It is not possible to obtain the net or absolute free energy of unfolding, ΔG_U, from pK_a shifts (*26*). The net electrostatic effects of charges can be determined so far only by continuum electrostatic calculations on the folded and unfolded structures (*28*, *29*). Calculations show, for example, that salt bridges are destabilizing the GCN4 leucine zipper because of a high desolvation penalty to be paid for dimerization (*30*). Both stabilizing and destabilizing salt bridges have been identified in leucine zipper Myc-Max (*31*).

We have recently completed structural and thermodynamic studies on the disulfide-linked heterodimeric AB_{SS} leucine zipper[2] composed of an acidic and a basic chain in which all *e* and *g* positions are occupied by either Glu in the A chain or Lys and Arg in the B chain (Figure 1) (*12*, *32*, *33*). Six interchain salt bridges are seen in the NMR structures of disulfide-linked AB_{SS}. However, Glu charges are destabilizing the coiled coil structure as indicated by most Glu pK_a^F values being upshifted in folded AB_{SS}, which is more stable at acidic pH where Glu side chains are uncharged. Mutational studies show that the salt bridges exist in AB_{SS} even if the Glu charges are destabilizing (*22*), in agreement with other studies revealing formation of destabilizing salt bridges (*28*, *30*, *31*, *34*, *35*).

In this paper, we present the NMR structures, the pH-dependent thermal stability profile, and the pK_a values of Glu and His residues of the homologous, non-disulfide-linked leucine zipper AB (Figure 1). We reasoned that the breakage of the disulfide bond between the acidic and basic chains should affect the pH stability profile. While the electrostatic environment in folded AB should be similar to that in folded AB_{SS}, it might differ in the unfolded states of the two proteins. In unfolded AB_{SS}, unfavorable charge repulsion among like charges and desolvation can be compensated by favorable charge attraction to opposite charges on the other, disulfide-linked chain. This is not possible for unfolded AB, which dissociates upon unfolding into separate A and B chains. Indeed, we find that residual electrostatic interactions destabilize the unfolded AB zipper but not the unfolded AB_{SS} zipper. As a consequence, electrostatic interactions, and interchain salt bridges in particular, contribute more to the relative stability of folded AB than to folded AB_{SS} despite the fact that the NMR structures of the two coiled coils are very similar. The results were obtained by direct determination of pK_a values using NMR spectroscopy and are supported by continuum electrostatic calculations.

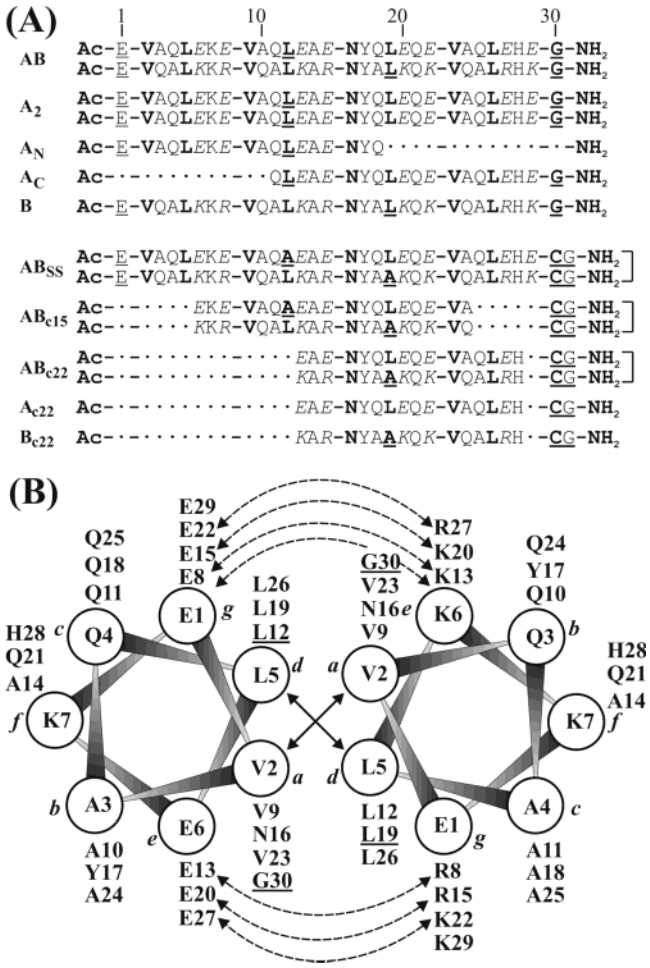

FIGURE 1: Primary sequences of heterodimeric leucine zipper AB, of homologous disulfide-linked leucine zipper AB_{SS}, and of unfolded reference peptides. (A) AB is a non-disulfide-linked coiled coil consisting of acidic chain A and basic chain B. A_N, A_C, B, A_{c22}, and B_{c22} are monomeric reference peptides modeling the unfolded states of the A and B chains. A_2 is the homodimeric leucine zipper of chain A formed at acidic pH. AB_{SS}, AB_{c15}, and AB_{c22} are the disulfide-linked coiled coil and its corresponding dimeric unfolded reference peptides, respectively (*22*). Heptad repeats are separated by dashes; *a* and *d* heptad position residues are in boldface, and *e* an *g* heptad position residues are in italics. Disulfide bridges are highlighted with brackets. Residues mutated in AB relative to AB_{SS} are underlined. (B) Helix wheel representation of the parallel aligned coiled coil AB. Heptad positions are denoted with lowercase letters in italics. Solid arrows denote hydrophobic interchain contacts of *a* and *d* heptad position residues at the chain interface. Dashed arrows denote interchain salt bridge formation between *g* and *e′*(+1) heptad position residues of chains A (left) and B (right).

EXPERIMENTAL PROCEDURES

Peptide Synthesis and Purification. Solid-phase peptide synthesis and purification have been described (*12*). Electrospray mass analyses of A and B chains yielded correct

[2] Abbreviations: 2D, two-dimensional; AB zipper, heterodimeric coiled coil consisting of Ac-EVAQLEKEVAQLEAENYQLEQEVAQLEHEG-NH_2 and Ac-EVQALKKRVQALKARNYALKQKVQALRHKG-NH_2 peptides; AB_{SS} zipper, disulfide-linked AB zipper containing L12A (acidic chain), L19′A (basic chain), and G30C (both chains) mutations; CD, circular dichroism; CDIH, dihedral angle restraint; COSY, 2D chemical shift-correlated spectroscopy; DF, double-quantum-filtered; EM, energy minimization; HSQC, heteronuclear single-quantum coherence; pK_a^F, equilibrium proton association constant in the folded state; pK_a^U, equilibrium proton association constant in the unfolded state; MD, molecular dynamics; NOE, nuclear Overhauser effect; NOESY, 2D NOE correlated spectroscopy; pH*, glass electrode pH reading, uncorrected for the deuterium isotope effect; RT, room temperature; θ, ellipticity; TOCSY, 2D total correlation spectroscopy; rmsd, root-mean-square deviation; sc, side chain; τ_{mix}, mixing time; vdW, van der Waals.

masses of 3495.8 and 3515.2 Da, respectively. Expected masses of 2132.3, 2398.5, 2219.4, and 2171.6 Da were determined for reference peptides A_N, A_C, A_{c22}, and B_{c22}, respectively. The latter two peptides included *S*-(*tert*-butylthio)Cys in position 30 (Figure 1).

CD Spectroscopy. Spectra were measured as described previously (*22*). Heterodimeric AB or homodimeric A_2 was formed by dissolving the peptide chains at 18.6 μM in buffer composed of boric, citric, and phosphoric acid, each at 7.5 mM. The pH was adjusted with KOH or HCl and the ionic strength fixed at 0.1 M with KCl. Thermal unfolding was performed as described previously (*22*) and was >90% reversible at any pH.

Analysis of Thermal Unfolding CD Traces of Heterodimeric AB and Homodimeric A_2. Temperature-dependent $[\theta_{222}]$ values were analyzed according to a two-state thermodynamic model in which temperature-dependent folded and unfolded fractions of the protein, $f_D(T)$ and $f_U(T)$, respectively, coexist. The equilibrium constant of unfolding, $K_U(T)$, of the AB heterodimer is defined as

$$K_{U,AB}(T) = \frac{[A][B]}{[AB]} = \frac{[1 - f_D(T)]^2 C_{tot}}{2 f_D(T)} \quad (1a)$$

where C_{tot} is the total protein concentration ($[A]_{tot} + [B]_{tot}$). The equilibrium constant of unfolding of the A_2 homodimer is

$$K_{U,A2}(T) = \frac{[A]^2}{[A_2]} = \frac{2[1 - f_D(T)]^2 C_{tot}}{f_D(T)} \quad (1b)$$

where C_{tot} is the total protein concentration ($[A]_{tot}$). The observed temperature-dependent ellipticity $\theta_{obs}(T)$ is related to $f_D(T)$ by

$$\theta_{obs}(T) = f_D(T)[\theta_D(0) + m_D T] + [1 - f_D(T)][\theta_U(0) + m_U T] \quad (2)$$

where $\theta_D(0)$ and $\theta_U(0)$ are the ellipticities of the folded and unfolded protein, respectively, at the reference temperature (0 °C) and m_D and m_U are the slopes of the linear temperature dependence of the ellipticities of the folded and unfolded forms, respectively. In case of the AB heterodimer, the dependence of $f_D(T)$ on the Gibbs free energy of unfolding $\Delta G_U(T)$ is described by

$$f_D(T) = \left[C_{tot} + \exp\left[\frac{-\Delta G_U(T)}{RT}\right] - \sqrt{\exp\left[\frac{-2\Delta G_U(T)}{RT}\right] + 2C_{tot}\exp\left[\frac{-\Delta G_U(T)}{RT}\right]} \right] \Big/ [C_{tot}] \quad (3a)$$

In case of the A_2 homodimer, the correlation is

$$f_D(T) = \left[4C_{tot} + \exp\left[\frac{-\Delta G_U(T)}{RT}\right] - \sqrt{\exp\left[\frac{-2\Delta G_U(T)}{RT}\right] + 8C_{tot}\exp\left[\frac{-\Delta G_U(T)}{RT}\right]} \right] \Big/ [4C_{tot}] \quad (3b)$$

$\Delta G_U(T)$ is expressed by the Gibbs−Helmholtz equation:

$$\Delta G_U(T) = \Delta H_U(T_m)[1 - T/T_m] + \Delta C_p[T - T_m - T\ln[T/T_m]] - RT\ln K_U(T_m) \quad (4)$$

where T_m is the transition midpoint temperature, $\Delta H_U(T_m)$ is the apparent transition enthalpy of unfolding at T_m, and ΔC_p is the difference in the heat capacity between the folded and unfolded states. A nonlinear fitting routine on combined eqs 2−4 was applied to simultaneously determine parameters $\Delta H_U(T_m)$, T_m, $\theta_D(0)$, $\theta_U(0)$, and m_D. m_U was assumed to be zero, and ΔC_p was set to 2.5 kJ mol^{-1} K^{-1} as established in earlier studies with AB_{SS} (*12*, *32*). Using the same ΔC_p that was used for AB_{SS} was justified since the solvent accessible surfaces of the NMR structures of AB and AB_{SS} are almost identical. The fitted T_m was verified by a minima search in the first derivative of combined eqs 2−4.

Correction for the Presence of Homodimeric A_2 at Low pH. At acidic pH, AB and A_2 coexist, precluding the analysis of unfolding CD traces with eqs 2−4. Nonetheless, ΔG_U(37 °C) of AB could be determined since (i) AB is exclusively formed at pH 7 and 37 °C, (ii) no B_2 dimer exists, (iii) free A is negligible at 37 °C, and (iv) $[\theta]_{222}$ values of folded AB and A_2 are very similar and independent of pH. The total fraction of dimer at acidic pH can be defined as

$$f_D = \frac{2([AB] + [A_2])}{C_{tot}} \quad (5a)$$

where C_{tot} is the total protein concentration ($[A]_{tot} + [B]_{tot}$, where $[A]_{tot} = [B]_{tot}$). Note that according to eq 5a, $f_D < 1$ if A_2 is formed and there is free B.

At 37 °C, f_D is described by

$$f_{D,37\,°C} = [\theta_{pH}(96\,°C) - \theta_{pH}(37\,°C)]/[\theta_{pH\,7}(96\,°C) - \theta_{pH\,7}(37\,°C)] \quad (5b)$$

[AB], [B], and $[A_2]$ are then estimated by

$$[AB] = (2f_{D,37\,°C} - 1)C_{tot}/2 \quad (6a)$$

$$[B] = (1 - f_{D,37\,°C})C_{tot} \quad (6b)$$

$$[A_2] = (1 - f_{D,37\,°C})C_{tot}/2 \quad (6c)$$

The equilibrium constant of unfolding, $K_{U,AB}$(37 °C), of the AB dimer is defined by

$$K_{U,AB}(37\,°C) = \frac{\sqrt{K_{U,A_2}(37\,°C)[A_2]}[B]}{[AB]} \quad (7)$$

where $K_{U,A2}$ is the equilibrium constant of A_2 determined from thermal unfolding of A_2 alone.

NMR Data Acquisition and Processing. The A and B chains were dissolved in 400 μL of a 90% H_2O/10% D_2O mixture at 2.6 mM each and pH* 5.7. A_N, A_C, and chain B reference peptides were dissolved at 2.9 mM and pH* 6.0. NMR data were recorded in quadrature at 37 °C on a Bruker Avance DRX600 spectrometer operating at 600 MHz (^{1}H), and equipped with 5 mm BBI or TXI *z*-gradient probes. Amino acid spin system identification was accomplished on the basis of 2D DQF-COSY and 2D TOCSY (τ_m = 75 ms)

experiments. 2D NOESY spectra (various τ_m values between 50 and 250 ms) served for sequential assignment (AB zipper). 2D ROESY ($\tau_m = 400$ ms) was used to identify sequential connectivities in unfolded reference peptides A_N, A_C, and chain B (resonance assignments in the Supporting Information). NMR parameters were chosen as described previously (*22*). A natural abundance 2D $^1H-^{15}N$ HSQC (*36*) spectrum on the AB zipper was recorded with 512 transients and 46 complex points along t_1. Data were processed with FELIX version 2000 (Accelrys, San Diego, CA) as reported previously (*12*). t_1 data of the $^1H-^{15}N$ HSQC spectra were linearly predicted to 96 complex points.

Determination of pK_a Values by NMR. Nineteen TOCSY spectra in the pH range of 9−2 were acquired on AB at 37 °C as described in detail previously (*22*). Fourteen TOCSY spectra were recorded on A_N in the pH range of 7−2. Eighteen TOCSY spectra were acquired on A_C and on the B chain in the pH range of 9−2. pH values were measured before and after NMR data acquisition and were consistent within 0.05 pH unit. The pH dependence of Glu $H^{\gamma/\gamma'}$ and His $H^{\delta 2/\epsilon 1}$ chemical shifts was interpreted according to

$$\delta(\mathrm{pH}) = \frac{\delta_a + \delta_b\, 10^{n(\mathrm{pH}-\mathrm{p}K_a)}}{1 + 10^{n(\mathrm{pH}-\mathrm{p}K_a)}} \qquad (8)$$

where δ_a and δ_b are the chemical shift plateaus at the acidic and basic pH limits, respectively, and n is the Hill coefficient (*37*). δ_a, δ_b, and pK_a were nonlinearly fitted, either including n as an additional fitting parameter to probe for cooperativity or fixing n at 1.

NMR-Derived Restraints and AB Structure Calculation. A total of 1987 cross-peaks were unambiguously assigned in the 2D NOESY spectrum; 1246 interproton distances were derived from the volume buildup in NOE experiments (τ_m = 50, 100, and 150 ms) by using the fixed separation of vicinal H^β and amide protons for the calibration of the distances according to the r^{-6} relationship between NOE volumes and proton separation. Upper limits of distances were established by adding 30% of the estimated distances after appropriate correction for pseudoatoms (*38*), and the lower limits were set to 1.8 Å. Three hundred five distances are between backbone protons, 627 between backbone and side chain protons, and 314 between side chain protons. Five hundred eight intraresidual, 284 sequential, 316 medium-range ($1 < |i - j| < 5$), and 138 interchain[3] long-range ($5 \leq |i - j|$) NOE connectivities were assigned.

A $^3J_{HN\alpha}$ of <6 Hz was identified as described previously (*12*) in the case of 44 residues, for which Φ torsion angles were restrained to $-60 \pm 30°$. Stereospecific assignment of β-protons of *a* and *d* position residues as well as stereospecific assignment of Val γ-methyl groups and identification of the Val *trans* χ_1 conformation was derived as reported previously (*12*).

Fifty AB zipper structures were calculated with CNS version 1.1 (*39*) using an implemented distance geometry/simulated annealing protocol previously applied for the calculation of the AB_{SS} NMR structures (*22*). The quality of the calculated structures was examined with PROCHECK-NMR version 3.4.4 (*40*), WHAT IF version 99 (*41*), MOLMOL version 2.6 (*42*), and CNS version 1.1 (*39*). The 50 calculated structures converged, showed good covalent geometry, and fulfilled the experimental restraints (Table 1). Low violation of experimental restraints and good agreement of pK_a^F values derived for the AB NMR structures by continuum electrostatic calculations with experimental Glu and His pK_a^F values were considered for selecting the 27 "best" structures. The backbone conformation of the selected AB zipper structures is of good quality: 88.7% of the Φ and Ψ angle pairs fall into the energetically most favored, 11.1% into additionally allowed, 0.2% into generously allowed, and none into disallowed areas of the Ramachandran plot.

Table 1: Structure Statistics of the AB Zipper

	ensemble of 50 structures	27 selected structures
rmsd from the mean of heavy atom coordinates[a]		
backbone (Å)	0.59 ± 0.23	0.59 ± 0.20
all (Å)	1.11 ± 0.24	1.09 ± 0.22
rmsd of experimental restraints[b]		
NOE		
all (Å)	0.014 ± 0.006	0.014 ± 0.007
intraresidual (Å)	0.007 ± 0.005	0.007 ± 0.005
sequential (Å)	0.016 ± 0.005	0.017 ± 0.006
medium-range ($1 < \|i-j\| < 5$) (Å)	0.016 ± 0.007	0.016 ± 0.008
long-range ($5 \leq \|i-j\|$) (Å)	0.015 ± 0.009	0.015 ± 0.010
CDIH (deg)	0.20 ± 0.11	0.20 ± 0.12
rmsd of geometric terms[c]		
bonds (Å)	0.002 ± 0.001	0.002 ± 0.001
angles (deg)	0.34 ± 0.04	0.34 ± 0.04
impropers (deg)	0.18 ± 0.04	0.18 ± 0.04
average deviation of Glu/His pK_a values[d]	0.25 ± 0.16	0.18 ± 0.15

[a] Relative to the mean obtained by best-fit superimposition of backbone N, C^α, and C′ atoms of residues Leu^5-Leu^{26} and $Leu^{5'}-Leu^{26'}$. [b] Deviation from upper and lower limits of experimental distance and angle constraints. [c] By reference to the idealized covalent geometry as defined in the "protein-allhdg.param" force field implemented in CNS (*39*). [d] pK_a values were calculated by continuum electrostatic calculations on the ensemble of structures and compared to the pK_a determined by titration.

Molecular Dynamics Simulation of Unfolded Peptides A and B. Peptide chains A and B were generated with Insight II version 2000 (Accelrys). The peptides were individually immersed in a cubic TIP3P-model water box (*43*) with an edge length of 62 Å using CHARMM version 30b1 (*44*). The solvent energy was minimized in two rounds by the conjugate gradient method with the solute initially fixed and harmonically restrained thereafter. Leapfrog Verlet MD simulation runs at a constant pressure and a temperature of 310 K were carried out separately with both solvated peptides for 20 ps, with the backbone of the solute harmonically restrained. Subsequent MD simulation runs on unrestrained solute were carried out for a total of 2 ns with snapshots of coordinates saved every 20 ps. Periodic boundaries on the water box were applied. Bonds involving protons were restrained by the shake command. Parameters were read from the force field "par_all22_prot.inp". The vdW energy term was modeled by a switched function effective in the range between 7.5 and 8.5 Å, and the electrostatic interactions were calculated using the particle mesh Ewald algorithm. Calculations were performed in parallel mode on a Silicon Graphics

[3] Twenty-one NOEs were identified between positions *a* and *a*′, 15 between positions *a* and *d*′, 24 between positions *a* and *d*′(−1), 17 between positions *a* and *g*′(−1), 15 between positions *d* and *d*′, and 46 between positions *d* and *e*′.

Origin platform. pK_a^U values were derived by continuum electrostatic calculations on the MD structures.

pK_a Calculation on NMR and MD Structures. Methods of the calculation of pK_a values on the basis of protein structures have been reviewed (*26*, *45*−*50*). Changed (i) background interaction, (ii) desolvation, and (iii) direct charge−charge interaction energies when the ionizable isolated model compound residue is positioned in the specific environment of the folded or unfolded protein induce a shift in the proton association constant K_a. pK_a values of ionizable groups in the AB zipper NMR structures and in the reference peptides simulated by MD were calculated with WHAT IF (*41*), applying the implemented proton optimization method. A numerical solution to the Poisson−Boltzmann equation was derived with DelPhi II (*47*). Atom charges and radii were as defined in the OPLS force field (*51*), and parameters for the grid search were used as described previously (*50*). Solvent and protein dielectric constants were set to 80 and 4, respectively, and the ionic strength was fixed at 150 mM. For the calculation of ΔpK_a affected by term (iii), pH-dependent charge occupancies of ionizable residues were established by Monte Carlo simulation (*49*). Model compound pK_a values of 4.4, 6.3, 9.6, 10.4, and 12.0 were assigned to the side chains of Glu, His, Tyr, Lys, and Arg, respectively. On the basis of calculated electrostatic terms (i)−(iii) and the pK_a values of all titratable groups, the pH-dependent contributions of the charged acidic, basic, and salt-bridged residues to stability were determined (see the Supporting Information).

Calculation of the pH-Dependent Relative Free Energy of Unfolding from pK_a^U and pK_a^F Values. We have discussed the relationship between pK_a^U, pK_a^F, and ΔG_U in detail elsewhere (*26*). Briefly, the change in the free energy of unfolding ($\delta\Delta G_U$) induced by a shift in pH (δpH) is expressed by

$$\delta\Delta G_U = \int_{pH} 2.303RT(Q_U - Q_F)\,\delta pH \qquad (9a)$$

where Q_U and Q_F refer to the total charge of the protein in the unfolded and folded state, respectively (*27*, *45*), $Q_U = \sum_{i=1}^{j} q_U^i$, and $Q_F = \sum_{i=1}^{j} q_F^i$. The individual charges q_U^i and q_F^i are given by

$$q = \frac{-1}{1 + 10^{pK_a - pH}} \text{ and } q = \frac{1}{1 + 10^{pH - pK_a}} \qquad (9b)$$

where the first term relates to a negative charge and the second to a positive charge. The relative pH-dependent contribution to the protein stability of residue *i* is

$$\delta\Delta G_U^i = \int_{pH} 2.303RT(q_U^i - q_F^i)\,\delta pH \qquad (9c)$$

Integration of eq 9c over the entire pH range yields

$$\Delta\Delta G_U^i = \Delta G_{U,dp}^i - \Delta G_{U,p}^i = 2.303RT(pK_a^{U,i} - pK_a^{F,i}) \qquad (10a)$$

where $\Delta G_{U,dp}^i$ and $\Delta G_{U,p}^i$ refer to the protein carrying residue *i* in entirely deprotonated and protonated forms, respectively. Hence, $\Delta\Delta G_U^i$ is the difference in the contribution of the fully charged versus the fully uncharged acidic residue *i* to the pH-dependent stability profile of the protein, and vice versa in case of a basic residue. If $pK_a^{U,i} > pK_a^{F,i}$, $\Delta\Delta G_U^i > 0$: the deprotonated form of residue *i* (charged Glu or uncharged His in AB) is more stabilizing than the protonated form. That means, a downshifted pK_a^F in folded AB or AB_{SS} indicates a favorable effect by charged Glu or uncharged His.

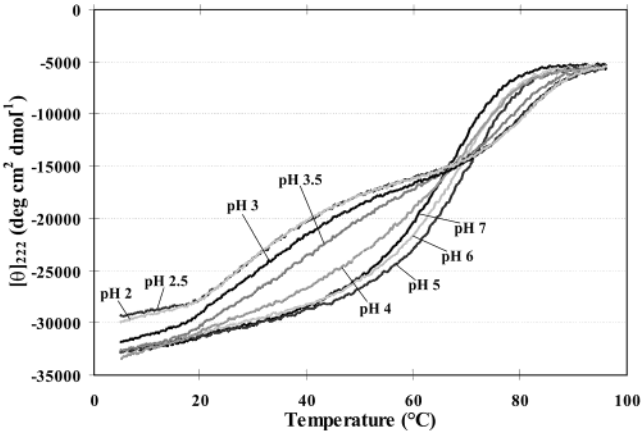

FIGURE 2: CD thermal unfolding traces of the AB zipper acquired between pH 2 and 7. The A and B chains were dissolved at 18.6 μM each, and the ionic strength was fixed at 0.1 M. Two transitions are apparent below pH 4.25 reflecting the melting of the AB heterodimer and the A_2 homodimer. No A_2 is formed above pH 4.25 because of charge−charge repulsion. Thermodynamic parameters of AB and A_2 are listed in Table 2.

Integration over all ionizable residues yields

$$\Delta\Delta G_U = \Delta G_{U,dp} - \Delta G_{U,p} = \sum_{i=1}^{j}(\Delta G_{U,dp}^i - \Delta G_{U,p}^i) = 2.303RT\sum_{i=1}^{j}(pK_a^{U,i} - pK_a^{F,i}) \qquad (10b)$$

Here, $\Delta\Delta G_U$ is the stability difference between the pH limits at which the protein is entirely protonated and deprotonated, respectively. $\sum_{i=1}^{j}(pK_a^{U,i} - pK_a^{F,i})$ is the sum of the pK_a shifts induced by unfolding.

RESULTS AND DISCUSSION

Leucine zipper AB is based on a sequence motif of the yeast transcriptional activator GCN4 (*12*). The A and B chain sequences of zipper AB are identical to those of the disulfide-linked leucine zipper AB_{SS} except for C30G, C30′G, A12L, and A19′L mutations (Figure 1). The former two mutations remove the S−S bond; the latter two strengthen the hydrophobic interface between the chains to compensate for the missing disulfide bridge.[4]

Thermal Unfolding of Non-Disulfide-Linked Zipper AB Indicates Stabilization by Charged Glu Residues. Because of the opposite net charges on the A and B chains at neutral pH, only the AB heterodimer is formed in the pH range of 4.25−8. Thermal unfolding traces above pH 4 had a single transition characteristic of two-state unfolding of a single molecular species (Figure 2) and are described by eqs 2−4. At acidic pH, repulsion between charged A chains is canceled through protonation of Glu side chains and A_2 homodimers

[4] Without strengthening of the hydrophobic interface by mutations A12L and A19′L, ΔG_U(20 °C, pH 7) of AB is only 20 kJ/mol (P. Phelan and H. R. Bosshard, unpublished data).

Table 2: Thermodynamic Parameters of the Heterodimeric AB and Homodimeric A_2 Zippers Established by Thermal Unfolding (pH Dependence of T_m, $\Delta H_U(T_m)$, and ΔG_U(37 °C) at an Ionic Strength of 0.1 M)

	T_m (°C)[a]		$\Delta H_U(T_m)$ (kJ/mol)[a]		ΔG_U(37 °C) (kJ/mol)[b]	
pH	AB	A_2[c]	AB	A_2[c]	AB[d]	A_2[c]
7.81 ± 0.03	66.1 ± 0.1		217.4 ± 5.4		45.3 ± 2.3	
7.41 ± 0.02	66.6 ± 0.1		214.6 ± 5.4		45.2 ± 2.3	
6.99 ± 0.01	67.1 ± 0.1		214.3 ± 5.4		45.4 ± 2.3	
6.50 ± 0.01	68.1 ± 0.1		217.5 ± 5.4		46.0 ± 2.3	
5.98 ± 0.02	69.3 ± 0.4		228.3 ± 5.7		47.5 ± 2.4	
5.48 ± 0.01	70.7 ± 0.1		227.4 ± 5.7		47.9 ± 2.4	
4.99 ± 0.01	70.9 ± 0.1		234.0 ± 5.9		48.6 ± 2.4	
4.50 ± 0.01	69.4 ± 0.1		241.8 ± 6.0		48.8 ± 2.4	
4.26 ± 0.01	68.9 ± 0.1		229.3 ± 5.7		47.4 ± 2.4	
4.02 ± 0.01		72.9 ± 0.1		265.3 ± 6.6	47.4 ± 2.4	50.9 ± 2.5
3.53 ± 0.01		78.6 ± 0.1		290.5 ± 7.3	45.2 ± 2.3	56.2 ± 2.8
3.05 ± 0.01		80.7 ± 0.1		298.0 ± 7.5	43.6 ± 2.2	58.0 ± 2.9
2.49 ± 0.03		81.5 ± 0.1		291.6 ± 7.3	42.0 ± 2.1	57.5 ± 2.9
2.04 ± 0.02		81.7 ± 0.1		299.9 ± 7.5	42.8 ± 2.1	58.7 ± 2.9

[a] Nonlinear least-squares fitting to combined eqs 2−4 of two independently measured CD thermal unfolding traces. [b] Values of ΔG_U(37 °C) were calculated according to eq 4 using fitted T_m and $\Delta H_U(T_m)$ and a ΔC_p of 2.5 kJ mol^{-1} K^{-1} (*32*). [c] From independent experiments with A chain alone. [d] ΔG_U(37 °C) values of the AB zipper below pH 4.25 are corrected for the presence of the A_2 homodimer (eqs 5−7); a 5% error for $\Delta H_U(T_m)$ and a 10% error of ΔG_U(37 °C) are estimates. The error in pH reflects differences in pH readings before and after thermal unfolding.

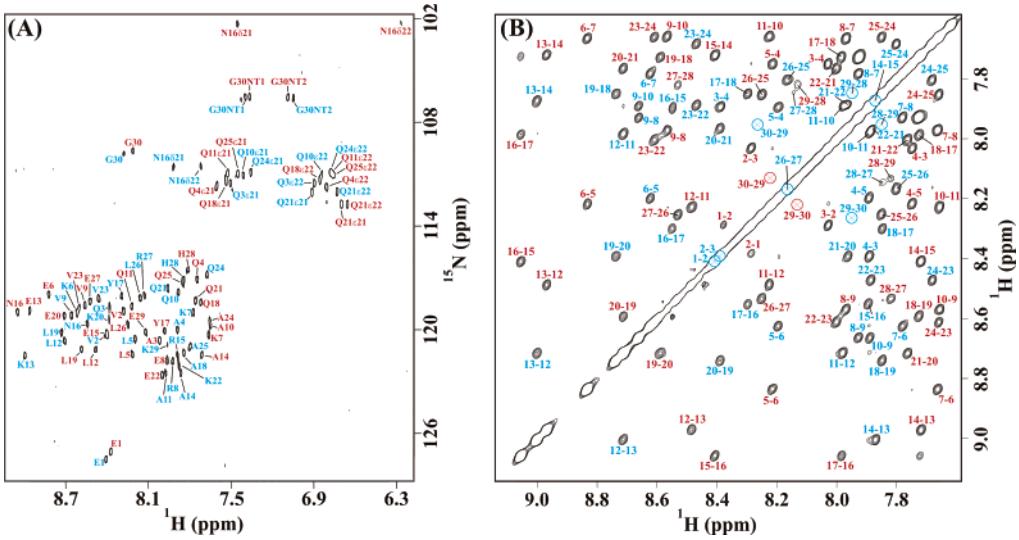

FIGURE 3: Sections of the natural abundance $^1H-^{15}N$ NMR 2D HSQC and the ^1H NMR 2D NOESY spectra acquired on the AB zipper. (A) Labeled cross-peaks connect $H^N_{(i)}$ to $N_{(i)}$ or side chain $H^{\delta21/\delta22/\epsilon21/\epsilon22}$ to $N^{\delta/\epsilon}$ within residues of the acidic (red labels) and basic (blue labels) chains. (B) Labeled cross-peaks in the amide region of the NOESY spectrum reveal connectivities between $H^N_{(i)}$ and $H^N_{(i+1)}$ of the acidic (red labels) and basic (blue labels) chains. Numbers denote proton pairs using the matrix convention (column proton−row proton). Missing or diagonal $H^N_{(i)}-H^N_{(i+1)}$ cross-peaks are represented by ⊗. Cross-peaks connecting $H^N_{(i)}$ to $H^N_{(i+2,i+3)}$ are not visible at the selected contour level. See Experimental Procedures for experimental details.

are being formed (*15*). Therefore, the AB heterodimer and the A_2 homodimer coexist at pH <4. The unfolding traces show two transitions, one for AB at lower temperatures and one for A_2 at higher temperatures (Figure 2). Unfolding of AB in the presence of A_2 below pH 4 was analyzed with eqs 5−7 and using parameters for A_2 determined in separate experiments.

Thermodynamic parameters obtained from thermal unfolding are given in Table 2. The stability of AB expressed as $\Delta G_{U,AB}$(37 °C) peaks at pH 4.5−5 and is higher at the basic than at the acidic pH limit, indicating favorable energy contributions from Glu charges. This is in contrast to our previous findings on disulfide-linked AB_{SS} whose stability is highest at pH 2 and decreases with increasing pH, in agreement with a a net destabilizing effect of Glu charges (*22*, *32*; see Figure 6).

NMR Structures of AB and AB_{SS} Are Similar. Proton resonances of amino acid spin systems of AB have been identified. The area in the 2D TOCSY and $^1H-^{15}N$ HSQC spectra show complete sets of well-resolved cross-peaks connecting $H^N_{(i)}$ to $H^\alpha_{(i)}$ and to ^{15}N, respectively (Figure 3A). Sequential assignment of the residues was achieved by identifying NOEs between $H^N_{(i)}$ and $H^N_{(i+1)}$ or between $H^N_{(i)}$ and $H^\alpha_{(i-1)}/H^\beta_{(i-1)}$ (Figures 3B and 4). α-Helical secondary structure of the A and B chains is evident from the NOEs between $H^\alpha_{(i)}$ and $H^N_{(i+3,i+4)}$, between $H^N_{(i)}$ and $H^N_{(i+1,i+2)}$, and between $H^\alpha_{(i)}$ and $H^\beta_{(i+3)}$ (*52*) (Figure 4). Furthermore, most H^α and ^{15}N resonances are distinctly high-field shifted in comparison with chemical shifts identified in a random coil structure (*53*), corroborating the formation of α-helices. The likelihood of α-helix formation is diminished in the C-

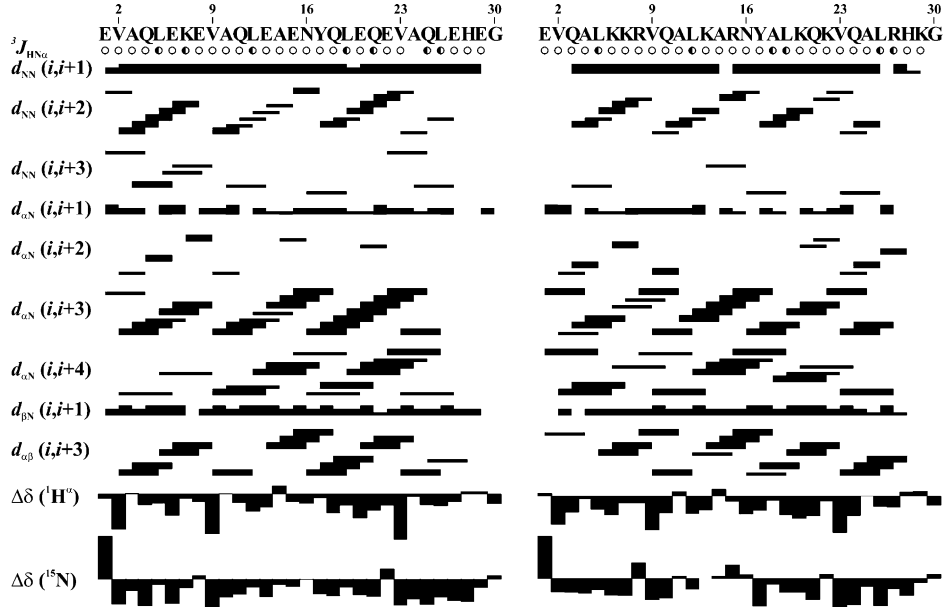

FIGURE 4: Overview of $^3J_{HN\alpha}$ couplings, backbone proton NOEs, and $H^\alpha/^{15}N$ chemical shift changes for the AB zipper. The sequences of the acidic (left) and basic (right) chains are shown. Half-filled and empty circles indicate H^N-H^α couplings ($^3J_{HN\alpha}$) of 6−8 and ≤6 Hz, respectively, measured in the DQF-COSY spectrum. Volume buildups of cross-peaks connecting $H^N_{(i)}$ to $H^N_{(i+1,i+2,i+3)}$, $H^\alpha_{(i)}$ to $H^N_{(i+1,i+2,i+3,i+4)}$, $H^\beta_{(i)}$ to $H^N_{(i+1)}$, and $H^\alpha_{(i)}$ to $H^\beta_{(i+3)}$ were measured in 2D NOESY spectra acquired with a τ_m between 50 and 150 ms. Bar widths represent the relative NOE cross-peak intensities. $\Delta\delta(H^\alpha)$ and $\Delta\delta(^{15}N)$ are the chemical shift changes of H^α and ^{15}N, respectively, in AB relative to the random coil structure (*53*).

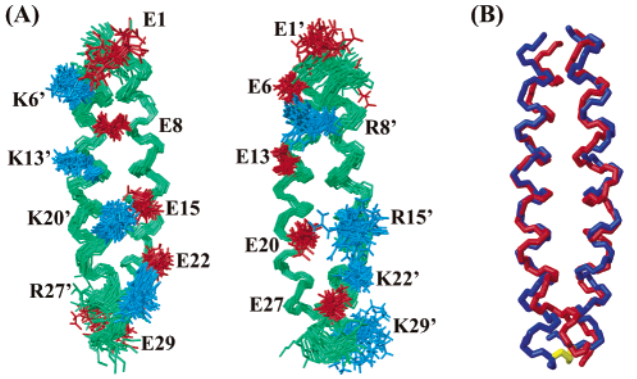

FIGURE 5: Alignment of ionizable residues in the ensemble of 27 AB NMR structures and superimposed backbone traces of the AB and AB_{SS} mean structures. (A) Side chain bonds and backbone traces of 27 selected AB NMR structures superimposed by fitting backbone heavy atoms (N, C^α, and C′) of residues 5−26 of both chains to the mean. Acidic residues are colored red and basic residues blue, and the backbone is colored green. Front and back views of AB are shown. (B) Superimposed mean structures of zipper AB (red) and zipper AB_{SS} (blue). The disulfide bond in AB_{SS} is colored yellow.

terminal region starting from residue 26(′) since the typical NOEs are weak or missing, and H^α chemical shifts are like those in the random coil conformation. $^3J_{HN\alpha}$ values of <6 Hz were identified for 44 residues, indicative of backbone Φ torsion angles characteristic of α-helical structure (*54*).

From 50 calculated structures, 27 structures were selected on the basis of little deviation of experimental restraints, including structure-derived Glu and His pK_a^F values obtained by continuum electrostatic calculations (Table 1). Hence, the conformational space occupied by the His and Glu side chains shown in Figure 5A is established by an additional experimental criterion, the pK_a^F value. The alignment of the side chains is imposed by NOEs linking *g* position residues to *d*, *f*, *a*(+1), *d*(+1), and *a*′(+1) position residues, the latter on the adjacent chain.[5] In case of *e* position residues, NMR-derived distance restraints reveal closeness to *a*, *b*, *d*, and *f* position residues of the same, and *d*′ position residues of the bound chain.[5] As a result, oppositely charged residues in *g* and *e*′(+1) positions are oriented toward one another and tend to form salt bridges. The averaged distance between heavy atoms of side chain functional groups of salt bridges is 1.1 ± 0.7 Å larger in AB than in AB_{SS} (*22*). This hints at a less tight hydrophobic packing and higher conformational flexibility of *e* and *g* position residues in the non-disulfide-linked dimer. A likely reason for the weaker interplay is the missing disulfide bond in AB: constriction of the A and B chains by the S−S bridge enhances the apparent local chain concentration to a constant value of ∼20−30 mM. Compared to that in AB, the apparent increase in chain concentration of 1 order of magnitude will further shift the equilibrium toward the folded structure in the case of AB_{SS}. Since structural restraints detected by NMR are averaged over a millisecond time range, larger distances result for non-disulfide-linked AB.

Mean NMR structures of AB and disulfide-linked AB_{SS} (*22*) are similar (Figure 5B). Alignment of N, C^α, and C′ backbone atoms of the averaged AB and AB_{SS} structures yields an rmsd of 1.2 Å for residues 5−26 of both chains. The largest differences are encountered at the C-terminal ends where the chains are covalently linked in AB_{SS} and the helical conformation is better preserved.

Determination of pK_a^F Values in the AB Zipper. pK_a^F values of all Glu side chain carboxylate groups and of His imidazole rings in the AB zipper have been derived from

[5] Seventy-one such intrachain and 26 interchain NOEs were observed for side chains of *e* position residues, and 46 intrachain and 15 interchain NOEs were identified for side chains of *g* position residues.

Table 3: Glu and His Side Chain pK_a Values of the Folded AB and AB_{SS} Leucine Zippers and of Unfolded Reference Peptides Determined by ^{1}H NMR at 37 °C, and the Relative pH-Dependent Contribution to the Stability $\Delta\Delta G_U$ Derived from ΔpK_a Induced by Unfolding

	AB	A_N, A_C, chain B			AB_{SS}[a]	AB_{c15}, AB_{c22}[a]			
residue	pK_a^F[b]	pK_a^U in reference peptides[b]	ΔpK_a[c]	$\Delta\Delta G_U$ (kJ/mol)[d]	pK_a^F[b]	pK_a^U in reference peptides[b]	ΔpK_a[c]	$\Delta\Delta G_U$ (kJ/mol)[d]	$\Delta\Delta\Delta G_U$[e]
E^1	4.10 ± 0.04	4.55 ± 0.03[f]	0.45 ± 0.05	2.67 ± 0.30	3.97 ± 0.03	4.35[i]	0.38 ± 0.03	2.26 ± 0.18	0.41 ± 0.35
E^6	4.90 ± 0.05	4.59 ± 0.14[f]	−0.31 ± 0.15	−1.84 ± 0.89	4.91 ± 0.02	4.29 ± 0.03	−0.62 ± 0.04	−3.68 ± 0.24	1.84 ± 0.92
E^8	4.89 ± 0.05	4.62 ± 0.10[f]	−0.27 ± 0.11	−1.60 ± 0.65	4.45 ± 0.02	4.33 ± 0.05	−0.12 ± 0.05	−0.71 ± 0.30	−0.89 ± 0.72
E^{13}	4.42 ± 0.08	4.70 ± 0.11[f]	0.28 ± 0.14	1.66 ± 0.83	4.34 ± 0.02	4.36 ± 0.15[j]	0.02 ± 0.15	0.12 ± 0.89	1.54 ± 1.22
E^{15}	4.09 ± 0.03	4.67 ± 0.13[f]	0.58 ± 0.13	3.44 ± 0.77	3.96 ± 0.03	4.31 ± 0.10[j]	0.35 ± 0.10	2.08 ± 0.59	1.36 ± 0.97
E^{20}	4.21 ± 0.04	4.61 ± 0.06[g]	0.40 ± 0.07	2.37 ± 0.42	4.41 ± 0.05	4.61 ± 0.11[j]	0.20 ± 0.12	1.19 ± 0.71	1.18 ± 0.82
E^{22}	4.83 ± 0.04	4.76 ± 0.09[g]	−0.07 ± 0.10	−0.42 ± 0.59	4.86 ± 0.03	4.53 ± 0.14[j]	−0.33 ± 0.14	−1.96 ± 0.83	1.54 ± 1.02
E^{27}	4.74 ± 0.01	4.58 ± 0.02[g]	−0.16 ± 0.02	−0.95 ± 0.12	4.65 ± 0.03	4.35 ± 0.02	−0.30 ± 0.04	−1.78 ± 0.24	0.83 ± 0.27
E^{29}	4.63 ± 0.02	4.63 ± 0.02[g]	0.00 ± 0.03	0.00 ± 0.18	4.67 ± 0.02	4.35[i]	−0.32 ± 0.02	−1.90 ± 0.12	1.90 ± 0.22
$E^{1'}$	4.24 ± 0.03	4.25 ± 0.01[h]	0.01 ± 0.03	0.06 ± 0.18	4.09 ± 0.04	4.35[i]	0.26 ± 0.04	1.54 ± 0.24	−1.48 ± 0.30
H^{28}	6.79 ± 0.01	6.65 ± 0.02[g]	−0.14 ± 0.02	−0.83 ± 0.12	6.83 ± 0.03	6.36 ± 0.03	−0.47 ± 0.04	−2.79 ± 0.24	1.96 ± 0.27
$H^{28'}$	6.34 ± 0.02	5.78 ± 0.01[h]	−0.56 ± 0.02	−3.32 ± 0.12	6.20 ± 0.02	6.24 ± 0.02	0.04 ± 0.03	0.24 ± 0.18	−3.56 ± 0.22
average Glu pK_a	4.51 ± 0.33	4.60 ± 0.14			4.43 ± 0.35	4.38 ± 0.10			
sum				1.24 ± 1.79				−5.39 ± 1.65	6.63 ± 2.44

[a] pK_a values from ref *22*. [b] pK_a values from fitting Glu $H^{\gamma/\gamma'}$ and His $H^{\delta 2/\epsilon 1}$ chemical shift data to eq 8. [c] $\Delta pK_a = pK_a^U - pK_a^F$. [d] $\Delta\Delta G_U = 2.303RT(pK_a^U - pK_a^F)$; a positive $\Delta\Delta G_U$ indicates that the deprotonated side chain (charged Glu and uncharged His) increases stability. [e] $\Delta\Delta\Delta G_U = \Delta\Delta G_U(AB) - \Delta\Delta G_U(AB_{SS})$; a positive $\Delta\Delta\Delta G_U$ indicates that the deprotonated side chain is more stabilizing in AB than in AB_{SS}. The sum $\sum\Delta\Delta\Delta G_U$ of 6.63 kJ/mol is indicated by a double-headed arrow in Figure 6. [f] pK_a^U of A_N. [g] pK_a^U of A_C. [h] pK_a^U of chain B. [i] Model pK_a since no experimental pK_a^U is available. [j] Mean pK_a^U of AB_{c15} and AB_{c22}.

the pH dependence of the $H^{\gamma/\gamma'}$ and $H^{\delta 2/\epsilon 1}$ chemical shifts (eq 8). The ionic strength varied between 20 and 100 mM during the course of the pH titration. The coiled coil structure was preserved from pH 9 to 2 as confirmed by NOESY experiments acquired at various pH values. Below pH 4, A_2 homodimer formation competes against AB heterodimerization as discussed above. However, at the high peptide concentration in the NMR pH titration experiment, the concentration of AB was at least 7 times that of A_2 and NMR signals of AB dominated over those of A_2 even at pH 2. Moreover, resonances of A_2 were weakened by intense peak broadening likely due to aggregation or slow conformational exchange of the A_2 dimer. Noteworthy is the fact that spectra recorded on similarly concentrated single-chain A at pH 2 were of poor quality.

Glu and His pK_a^F values of the AB heterodimer are listed in Table 3 and are similar to those determined previously for disulfide-linked AB_{SS} (*22*). pK_a^F values below 4.4, which is the model pK_a of a freely accessible, noninteracting Glu side chain (*55*), are seen for N-terminal Glu^1 and $Glu^{1'}$ interacting with the positively charged α-helix dipole, and for Glu^{15} and Glu^{20} that maintain ion pairing interactions with $Lys^{20'}$ and $Arg^{15'}$, respectively (Figure 5A). pK_a^F values significantly higher than the model pK_a of 4.4 are observed for Glu in positions 6, 8, 22, 27, and 29. The average Glu pK_a^F value is 0.08 pH unit higher in the AB zipper than in AB_{SS}, testifying to weaker electrostatic stabilization by charged Glu residues in AB. Indeed, the averaged distance between heavy atoms of side chain functional groups of salt bridges is larger in AB, consistent with the upshifted pK_a^F.

Determination of pK_a^U Values of Unfolded AB Represented by Peptides A_N, A_C, and Chain B. To calculate the energetic contribution of ionizable side chains, both pK_a^F and pK_a^U must be known (eq 10). Peptides A_N and A_C covering residues 1−18 and 11−30 of the A chain as well as the B chain were used to measure pK_a^U values. The former two peptides are too short to form coiled coils at acidic pH yet long enough to mimic the unfolded A chain. Folding of the B chain is prevented at any pH due to charge repulsion. NMR pH titrations were performed in the absence of the companion A and B chains to reduce the complexity of NMR spectra. This was justified since after unfolding, the dissociated A and B chains are sufficiently separated that they do not experience electrostatic interaction. In a 2.9 mM peptide solution used for NMR spectroscopy, the mean distance between the chains is ∼92 Å assuming that the peptides are statistically distributed in body- or face-centered cubic unit cells. It is noteworthy that pK_a^U values of His^{28}, $His^{28'}$, Glu^{27}, and Glu^{29} derived from titrations on peptide A_C or chain B alone and on a 1:1 mixture of A_C and B_{c22} were identical within error. This consistency demonstrates that electrostatic interactions are not biased by the absence of the companion chains in the titration. During titration, H^N resonances were bounded to an area ranging from 7.96 to 8.37 ppm in support of random coil conformation (*53*) (Figure 1 of the Supporting Information).

Glu pK_a^U values are shown in Table 3. Compared to a model pK_a of 4.4 for a noninteracting isolated Glu side chain, pK_a^U values of A_N and A_C are prominently upshifted. In contrast, pK_a^U value of $Glu^{1'}$ on chain B is downshifted. The average side chain pK_a^U of Glu in unfolded A_N, A_C, and chain B is 4.60 ± 0.14. This is significantly higher than the average pK_a^U of 4.38 ± 0.10 for Glu side chains in unfolded AB_{SS} [unfolded AB_{SS} was represented by disulfide-linked peptides AB_{c15} and AB_{c22} shown in Figure 1 (*22*)]. One might argue that the upshifted pK_a^U values of the AB reference peptides are caused by sequential differences between the acidic chains of AB and AB_{SS}: Leu^{12} of A_C which is absent in AB_{c22} promotes hydrophobic interactions, leading to a more compact unfolded state and enhanced charge repulsion among Glu residues. However, pK_a^U values of reduced A_{c22} are upshifted to an extent similar to those of A_C (*22*). This is clear evidence for nonlocal favorable electrostatic interactions of the Glu with charged residues of the disulfide-linked

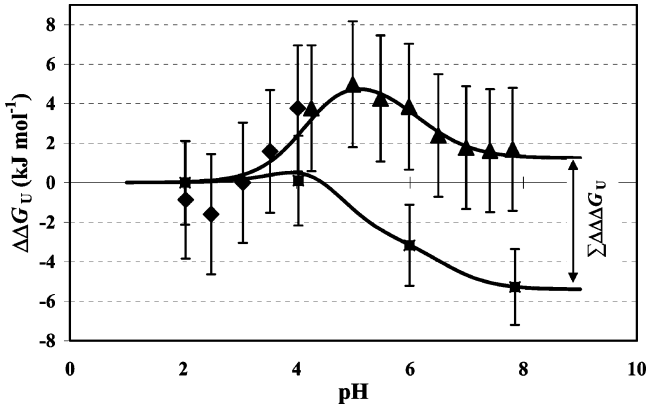

FIGURE 6: Relative pH-dependent stabilities of the AB and AB_{SS} leucine zippers. Stabilities are normalized to pH 2 according to the relation $\Delta\Delta G_U(pH) = \Delta G_U(pH) - \Delta G_U(pH\ 2)$ and refer to 37 °C. Symbols represent $\Delta\Delta G_U$ values from thermal unfolding (Table 2): [(■) AB_{SS}, (▲) AB above pH 4, and (◆) AB below pH 4.25 corrected for the formation of A_2]. Solid lines are calculated according to eqs 9a and 9b using values of pK_a^F and pK_a^U from Table 3. $\sum\Delta\Delta\Delta G_U$ is the normalized stability difference between AB and AB_{SS} at pH 8 as defined in Table 3.

basic chain in AB_{c22} compensating for unfavorable interchain repulsion which dominates in A_C and A_{c22}. His pK_a^U values of unfolded AB were estimated from titrations of peptides A_C and chain B. Compared to a pK_a of 6.3 of a freely accessible, noninteracting His, the pK_a^U of His^{28} is upshifted by ~0.3 pH unit, whereas that of $His^{28'}$ is downshifted by 0.5 pH unit (Table 3).

The Higher Stability of AB at Neutral pH Is Caused by Unfavorable Electrostatic Interactions in Unfolded A and B Chains. The mean pK_a^F of all the Glu residues in folded AB is 4.51, whereas the mean pK_a^F of Glu residues in AB_{SS} is only 4.43 (Table 3). Taken at face value, this should indicate an even lower stability at pH 8 relative to that at pH 2 for folded AB. Thermal unfolding shows the opposite: The relative stability of AB peaks at pH 4.5 and is higher at pH 8 than at pH 2, while the relative stability of AB_{SS} decreases with an increase in pH (Figure 6). Comparing the energetic effect of charges in unfolded AB and AB_{SS} solves this seeming contradiction. The mean pK_a^U of Glu residues in the reference peptides representing unfolded AB is 4.60; that of peptides AB_{c15} and AB_{c22} representing unfolded AB_{SS} is only 4.38 (Table 3). The latter value is typical of a freely accessible, noninteracting Glu side chain (*55*). The upshifted mean pK_a^U of unfolded AB points to energetically unfavorable electrostatic interactions between charged Glu side chains. *Therefore, the principal reason charged Glu side chains are stabilizing the AB zipper yet destabilizing the AB_{SS} zipper is an unfavorable environment of the charges in unfolded AB but not in unfolded AB_{SS}.* In other words, the higher stability of AB at neutral pH is not caused by stronger electrostatic attractions in folded AB but by unfavorable desolvation and stronger charge repulsions in unfolded AB.

If only the six residues (Glu^8, Glu^{13}, Glu^{15}, Glu^{20}, Glu^{22}, Glu^{27}) forming salt bridges in the NMR structures of AB are considered (Figures 1 and 5A), they stabilize the AB zipper by 4.5 kJ/mol (net) (charged Glu^{13}, Glu^{15}, and Glu^{20} contribute favorably and charged Glu^8, Glu^{22}, and Glu^{27} unfavorably). In disulfide-linked AB_{SS}, the same six Glu side chains form the same six interchain salt bridges but destabilize AB_{SS} by −1.1 kJ/mol (net) in the charged form (*22*). Again, it is the unfavorable environment of the six Glu residues in unfolded AB that renders the salt bridges relatively more stabilizing in the AB zipper; it is not because of stronger ionic interactions in folded AB.

What is the contribution of residues Glu^1, $Glu^{1'}$, Glu^6, and Glu^{29} that are not involved in salt bridges? Glu^1 and $Glu^{1'}$ interact with the positive α-helix dipole end and thus display downshifted pK_a^F values. Charged N-terminal Glu^1 of the acidic chain helps to stabilize AB, as in AB_{SS}. $Glu^{1'}$ of the basic chain "feels" the positive charges in the unfolded dissociated chain B, resulting in a downshifted pK_a^U comparable to pK_a^F. Therefore, the energy contribution of charged $Glu^{1'}$ is negligible in AB, contrasting its favorable contribution to the stability of AB_{SS}. Residues Glu^6 and Glu^{29} lack oppositely charged partner residues in the folded NMR structures of AB. Indeed, Glu^6 destabilizes AB by −1.8 kJ/mol; destabilization by Glu^{29} is negligible. However, in AB_{SS}, "lonely" residues Glu^6 and Glu^{29} together destabilize the structure by −5.6 kJ/mol (*22*). Once again, stronger destabilization of AB_{SS} is not due to stronger desolvation and charge−charge repulsion in the folded zipper but due to unfavorable interactions between charged Glu residues in unfolded AB.

Finally, the imidazole side chains of residues His^{28} and $His^{28'}$ play a crucial role in shaping the pH-dependent stability profile in the pH range of 5−8 (*22*). Charged His^{28} of the A chain is highly stabilizing AB_{SS} (−2.8 kJ/mol) but only moderately stabilizing AB (−0.8 kJ/mol). The situation is reversed for $His^{28'}$, which has a negligible effect in AB_{SS} (0.2 kJ/mol) yet stabilizes AB by −3.3 kJ/mol (note that the sign for stabilization by His is negative). Together, the charged His side chains are more stabilizing in the AB zipper mainly because charged His experiences an energetically unfavorable environment in the unfolded B chain.

We can now rationalize the different pH−stability profiles of AB and AB_{SS} shown in Figure 6 in terms of different electrostatic effects. Compared to pH 2, AB is more stable at pH 8 by 1.2 kJ/mol and AB_{SS} is less stable by −5.4 kJ/mol (calculated with eq 10b). Since both charged Glu and charged His are stabilizing the AB zipper and since Glu begins to be charged above pH 3 and His begins to lose its charge above pH 5.5, the stability of AB peaks near pH 4.5. In AB_{SS}, however, charged Glu is destabilizing and charged His is stabilizing. Therefore, the stability curve steadily decreases above pH 4, and no peak is apparent (Figure 6).

Calculation of Electrostatic Effects in Folded and Unfolded AB. We have calculated the electrostatic energies of ionizable residues in the ensemble of 27 NMR structures of folded AB and in a set of 100 unfolded structures of the A and B chains generated by MD simulation. Calculated pK_a values agree well with experimentally determined pK_a values. The rmsd of experimentally determined and calculated pK_a values is 0.18 ± 0.15 pH unit for folded AB and 0.15 ± 0.08 pH unit for unfolded AB (Table 9 of the Supporting Information). In the calculation, pK_a shifts refer to model compound pK_a values and are expressed by ΔpK_a^{total}, reflecting the energetic consequence of transferring an isolated and well-solvated ionizable model compound residue into the protein environment. ΔpK_a^{total} is affected by three electrostatic energy terms (*26*, *41*, *46*, *47*): (i) the background

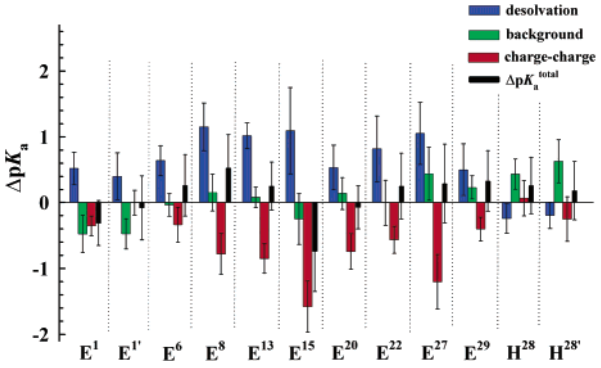

FIGURE 7: Changes of electrostatic free energy expressed as ΔpK_a induced by folding of the AB zipper. ΔpK_a values were computed for the ensemble of folded AB NMR structures and for unfolded structures of chains A and B generated by MD simulations. $\Delta pK_a = pK_a^F - pK_a^U$.[6] The total pK_a change, ΔpK_a^{total} (black bars), is composed of a direct charge−charge interaction term (red bars), a desolvation term (blue bars), and a background interaction term (green bars). Note that negative bars are favorable for charged Glu and unfavorable for charged His.

interaction of the charged residue with partial charges of permanent dipoles, (ii) the desolvation when moving the well-solvated ionizable group from the high-dielectric environment of the solvent to the low-dielectric environment of the solute where the residue is less solvated, and (iii) the direct charge−charge interaction with other ionizable groups in the protein. Terms (i) and (ii) are pH-independent and define the intrinsic pK_a. The last term is pH-dependent because it directly depends on the charge occupancies of the surrounding interacting ionizable groups (*49*).

The net unfavorable environment of charged Glu residues in the unfolded A and B chains is confirmed by the calculation. Partitioning yields net unfavorable desolvation, net unfavorable charge−charge interaction, and net favorable background interaction in MD-simulated unfolded A and B chains. The mean effects for Glu are as follows: ΔpK_a^U(desolvation) = 0.13 ± 0.04, ΔpK_a^U(charge−charge) = 0.01 ± 0.09, and ΔpK_a^U(background) = −0.06 ± 0.05 (amounting to $\Delta pK_a^{total} = 0.08 \pm 0.11$). Adding this value to a pK_a of 4.4 for a model Glu residue gives a mean pK_a^U of 4.48 ± 0.11 for all the Glu residues.

Single partitioned energies for individual Glu and His residues are illustrated in Figure 7. Bars in Figure 7 represent the relation $\Delta pK_a = pK_a^F - pK_a^U$, where pK_a^U was calculated for the MD structures of the unfolded A and B chains and pK_a^F for the NMR structures of AB.[6] The desolvation energy is always unfavorable, particularly for residues involved in ion pairing. A less well structured C-terminus of the AB zipper deduced by NMR could be reflected by the lower desolvation penalty paid by Glu^{29}, His^{28}, and $His^{28'}$. Background interactions of Glu tend to be favorable near

[6] Calculation actually yields the relations $\Delta pK_a^U = pK_a^U - pK_a$(model compound) and $\Delta pK_a^F = pK_a^F - pK_a$(model compound). Hence, it would be more appropriate to write $\Delta\Delta pK_a = \Delta pK_a^F - \Delta pK_a^U$. Since model compound pK_a values are canceled in $\Delta\Delta pK_a$, we have chosen the simpler nomenclature. Similarly, the ΔG(model compound) of charging the model compound is canceled in the calculation of $\Delta\Delta G_{U(uncharged-charged)}$ of Figure 8, justifying the simpler expression $\Delta\Delta G_{U(uncharged-charged)} = \Delta\Delta G_{folded} - \Delta\Delta G_{unfolded}$, where $\Delta\Delta G_{folded} = \Delta G_{folded}$(protein) − ΔG(model compound) and $\Delta\Delta G_{unfolded} = \Delta G_{unfolded}$(protein) − ΔG(model compound).

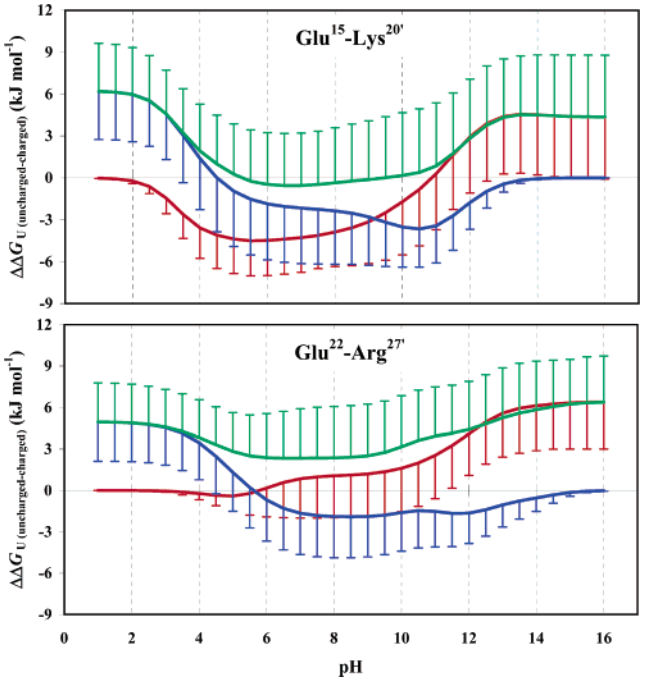

FIGURE 8: Calculated pH-dependent free energy contributions to the stability of AB by Glu^{15}−$Lys^{20'}$ and Glu^{22}−$Arg^{27'}$ salt bridges. Energy contributions of the single and paired charges were calculated for the ensemble of folded NMR ($\Delta\Delta G_{folded}$) and unfolded MD structures ($\Delta\Delta G_{unfolded}$) as explained in the Supporting Information. Results are expressed as $\Delta\Delta G_{U(uncharged-charged)} = \Delta\Delta G_{folded} - \Delta\Delta G_{unfolded}$.[6] Positive values represent unfavorable contributions of the charges. Contributions by Glu (red), Lys or Arg (blue), and the salt bridge (green) are shown. Errors were derived for the ensemble of NMR and MD structures.

the N-termini of the chains and unfavorable near the C-termini because of the α-helix dipole. For the same reason, His^{28} and $His^{28'}$ display favorable background energy terms. Except for $Glu^{1'}$, the direct charge−charge interactions are favorable for Glu residues, particularly for those forming salt bridges.

Energetic Contribution of Charges of Single Salt Bridges. We have calculated the pH-dependent contributions of charges of the Glu^{15}−$Lys^{20'}$ and Glu^{22}−$Arg^{27'}$ salt bridges to the stability (details in the Supporting Information). The two salt bridges were selected because the former negligibly affects the stability of the AB zipper and the latter is destabilizing. pK_a^F of Glu^{15} is depressed and that of Glu^{22} upshifted in folded AB (Table 3). The calculated contribution of the individual charges of Glu, Lys, and Arg is expressed as $\Delta\Delta G_{U(uncharged-charged)}$,[6] which is the difference between the contributions calculated for the unfolded and folded state (Figure 8). Charged Glu^{15} is stabilizing up to pH 11, i.e., as long as $Lys^{20'}$ and other basic residues carry positive charges (Figure 8, top). When these charges are lost at higher pH, charge repulsion among Glu side chains and desolvation make charged Glu^{15} unfavorable at high pH. Similarly, charged $Lys^{20'}$ is stabilizing above pH 4.5 and destabilizing below the point at which Glu side chains are being protonated. The net effect of the charged Glu^{15}−$Lys^{20'}$ pair is negligible in the pH range of 5−10 and unfavorable outside this pH range. Note that the net effect of the pair is not the sum of the effects of the individual charges because the direct charge interaction term of the pair is summed only once (*28*, *45*). In disulfide-linked AB_{SS}, the Glu^{15}−$Lys^{20'}$ pair desta-

bilizes the coiled coil structure by 5 kJ/mol at neutral pH (*22*). As discussed above, the switch from a destabilizing to a negligible role of the salt bridge charges is due to unfavorable charge effects in unfolded AB but not in unfolded AB_{SS}.

The charge of Glu^{22} of the $Glu^{22}-Arg^{27'}$ salt bridge is unfavorable over a wide pH range where the basic partner residue $Arg^{27'}$ is charged (Figure 8, bottom). The extent of destabilization pronouncedly increases above pH 10 where basic residues are becoming deprotonated. Charged $Arg^{27'}$ on the other hand is stabilizing above pH 5.5 and destabilizing at low pH when charged counterions are disappearing. The net effect of the charges of the $Glu^{22}-Arg^{27'}$ salt bridge is unfavorable at any pH, with a minimum of 2.3 kJ/mol at pH 6−8. In AB_{SS}, the same salt bridge is much more destabilizing, namely, by 5.3 kJ/mol (*22*). Again, unfavorable charge interactions in unfolded AB are responsible for the $Glu^{22}-Arg^{27'}$ salt bridge being less destabilizing in the AB zipper.

CONCLUSIONS

We have determined the NMR structure and the pH-dependent stability profile of the heterodimeric leucine zipper AB composed of an acidic and a basic chain and featuring six interchain salt bridges. The results were compared to those obtained before with the homologous, disulfide-linked leucine zipper AB_{SS} featuring the same six salt bridges (*12*, *22*, *32*).

Charged Glu side chains increase the relative free energy of unfolding of the leucine zipper AB at neutral pH. In contrast, the same set of charged Glu side chains decrease the relative stability of the homologous disulfide-linked leucine zipper AB_{SS} at neutral pH (*12*, *22*, *32*). At first sight, one could have concluded that charge−charge interactions are more favorable in folded AB and less favorable in folded AB_{SS}. This is, however, not the case. On the contrary, the mean pK_a^F value of the Glu side chains is slightly higher in the folded AB zipper than in folded AB_{SS}, which points to weaker electrostatic stabilization of folded AB by Glu charges. This is in accord with slightly larger distances between the heavy atoms of side chain functional groups forming salt bridges in AB when compared with distances for the same set of atoms in AB_{SS}. Therefore, a simple comparison of the *folded* states of AB and AB_{SS} does not explain the experimental observation but rather indicates the opposite: lower stability of AB at neutral pH relative to acidic pH. The reason for the higher relative stability of the non-disulfide-linked leucine zipper AB is clearly due to unfavorable electrostatic interactions in the unfolded A and B chains to which AB dissociates on denaturation. In other words, it is the remarkably higher free energy G_U of the unfolded state and not a lower free energy G_F of the folded protein that makes zipper AB relatively more stable at neutral pH. Such a pronounced electrostatic influence by the unfolded state we call an *inverse electrostatic effect* to emphasize the fact that the electrostatics of the unfolded state dominate the stability of the folded state. There are presumably several other instances of inverse electrostatic effects in proteins that went unnoticed because studies of protein stability are typically focused on the folded state.

ACKNOWLEDGMENT

We thank Dr. Ilian Jelesarov for helpful discussions and comments.

SUPPORTING INFORMATION AVAILABLE

Equations used for the calculation of the data depicted in Figure 8; four tables listing the chemical shifts of the AB zipper, the A_N and A_C reference peptides, and the B chain; four tables listing the parameters obtained by fitting pH-dependent chemical shift data of AB, A_N, A_C, and the B chain to the Henderson−Hasselbalch equation; a table listing pK_a values derived by continuum electrostatic calculations on structures of the AB zipper and of the unfolded A and B chains; and a figure showing the "fingerprint" area in the ^{1}H NMR TOCSY spectra recorded on A_N and A_C, respectively. This material is available free of charge via the Internet at http://pubs.acs.org.

REFERENCES

1. Elcock, A. H. (1999) Realistic modeling of the denatured states of proteins allows accurate calculations of the pH dependence of protein stability, *J. Mol. Biol. 294*, 1051−1062.
2. Whitten, S. T., and Garcia-Moreno, E. B. (2000) pH dependence of stability of staphylococcal nuclease: evidence of substantial electrostatic interactions in the denatured state, *Biochemistry 39*, 14292−14304.
3. Kuhlman, B., Luisi, D. L., Young, P., and Raleigh, D. P. (1999) pK_a values and the pH dependent stability of the N-terminal domain of L9 as probes of electrostatic interactions in the denatured state. Differentiation between local and nonlocal interactions, *Biochemistry 38*, 4896−4903.
4. Oliveberg, M., Arcus, V. L., and Fersht, A. R. (1995) pK_a values of carboxyl groups in the native and denatured states of barnase: the pK_a values of the denatured state are on average 0.4 units lower than those of model compounds, *Biochemistry 34*, 9424−9433.
5. Tan, Y. J., Oliveberg, M., Davis, B., and Fersht, A. R. (1995) Perturbed pK_a-values in the denatured states of proteins, *J. Mol. Biol. 254*, 980−992.
6. Tollinger, M., Crowhurst, K. A., Kay, L. E., and Forman-Kay, J. D. (2003) Site-specific contributions to the pH dependence of protein stability, *Proc. Natl. Acad. Sci. U.S.A. 100*, 4545−4550.
7. Crowhurst, K. A., and Forman-Kay, J. D. (2003) Aromatic and methyl NOEs highlight hydrophobic clustering in the unfolded state of an SH3 domain, *Biochemistry 42*, 8687−8695.
8. O'Shea, E. K., Klemm, J. D., Kim, P. S., and Alber, T. (1991) X-ray structure of the GCN4 leucine zipper, a two-stranded, parallel coiled coil, *Science 254*, 539−544.
9. Glover, J. N., and Harrison, S. C. (1995) Crystal structure of the heterodimeric bZIP transcription factor c-Fos-c-Jun bound to DNA, *Nature 373*, 257−261.
10. Junius, F. K., O'Donoghue, S. I., Nilges, M., Weiss, A. S., and King, G. F. (1996) High-resolution NMR solution structure of the leucine zipper domain of the c-Jun homodimer, *J. Biol. Chem. 271*, 13663−13667.
11. Lavigne, P., Crump, M. P., Gagne, S. M., Hodges, R. S., Kay, C. M., and Sykes, B. D. (1998) Insights into the mechanism of heterodimerization from the ^{1}H-NMR solution structure of the c-Myc-Max heterodimeric leucine zipper, *J. Mol. Biol. 281*, 165−181.
12. Marti, D. N., Jelesarov, I., and Bosshard, H. R. (2000) Interhelical ion pairing in coiled coils: solution structure of a heterodimeric leucine zipper and determination of pK_a values of Glu side chains, *Biochemistry 39*, 12804−12818.
13. Kohn, W. D., Kay, C. M., and Hodges, R. S. (1995) Protein destabilization by electrostatic repulsions in the two-stranded α-helical coiled-coil/leucine zipper, *Protein Sci. 4*, 237−250.
14. Jelesarov, I., and Bosshard, H. R. (1996) Thermodynamic characterization of the coupled folding and association of heterodimeric coiled coils (leucine zippers), *J. Mol. Biol. 263*, 344−358.
15. Durr, E., Jelesarov, I., and Bosshard, H. R. (1999) Extremely fast folding of a very stable leucine zipper with a strengthened

hydrophobic core and lacking electrostatic interactions between helices, *Biochemistry 38*, 870−880.
16. Jelesarov, I., Durr, E., Thomas, R. M., and Bosshard, H. R. (1998) Salt effects on hydrophobic interaction and charge screening in the folding of a negatively charged peptide to a coiled coil (leucine zipper), *Biochemistry 37*, 7539−7550.
17. O'Shea, E. K., Rutkowski, R., Stafford, W. F., III, and Kim, P. S. (1989) Preferential heterodimer formation by isolated leucine zippers from fos and jun, *Science 245*, 646−648.
18. Lavigne, P., Kondejewski, L. H., Houston, M. E., Jr., Sonnichsen, F. D., Lix, B., Skyes, B. D., Hodges, R. S., and Kay, C. M. (1995) Preferential heterodimeric parallel coiled-coil formation by synthetic Max and c-Myc leucine zippers: a description of putative electrostatic interactions responsible for the specificity of heterodimerization, *J. Mol. Biol. 254*, 505−520.
19. Lumb, K. J., and Kim, P. S. (1995) Measurement of interhelical electrostatic interactions in the GCN4 leucine zipper., *Science 268*, 436−439.
20. Lumb, K. J., and Kim, P. S. (1996) Interhelical salt bridges, coiled coil stablity, and specificity of dimerization, *Science 271*, 1137−1138.
21. Lavigne, P., Sonnichsen, F. D., Kay, C. M., and Hodges, R. S. (1996) Interhelical salt bridges, coiled-coil stability, and specificity of dimerization, *Science 271*, 1136−1137.
22. Marti, D. N., and Bosshard, H. R. (2003) Electrostatic interactions in leucine zippers: Thermodynamic analysis of the contributions of Glu and His residues and the effect of mutating salt bridges, *J. Mol. Biol. 330*, 621−637.
23. Zhou, N. E., Kay, C. M., and Hodges, R. S. (1994) The net energetic contribution of interhelical electrostatic attractions to coiled-coil stability, *Protein Eng. 7*, 1365−1372.
24. Krylov, D., Barchi, J., and Vinson, C. (1998) Inter-helical interactions in the leucine zipper coiled coil dimer: pH and salt dependence of coupling energy between charged amino acids, *J. Mol. Biol. 279*, 959−972.
25. Krylov, D., Mikhailenko, I., and Vinson, C. (1994) A thermodynamic scale for leucine zipper stability and dimerization specificity: *e* and *g* interhelical interactions, *EMBO J. 13*, 2849−2861.
26. Bosshard, H. R., Marti, D. N., and Jelesarov, I. (2004) Protein stabilization by salt bridges: concepts, experimental approaches and clarification of some misunderstandings, *J. Mol. Recognit. 17*, 1−16.
27. Tanford, C. (1970) Protein denaturation. C. Theoretical models for the mechanism of denaturation, *Adv. Protein Chem. 24*, 1−95.
28. Hendsch, Z. S., and Tidor, B. (1994) Do salt bridges stabilize proteins: a continuum electrostatic analysis, *Protein Sci. 3*, 211−226.
29. Schutz, C. N., and Warshel, A. (2001) What are the dielectric "constants" of proteins and how to validate electrostatic models? *Proteins 44*, 400−417.
30. Hendsch, Z. S., and Tidor, B. (1999) Electrostatic interactions in the GCN4 leucine zipper: substantial contributions arise from intramolecular interactions enhanced on binding, *Protein Sci. 8*, 1381−1392.
31. Kumar, S., and Nussinov, R. (2000) Fluctuations between stabilizing and destabilizing electrostatic contributions of ion pairs in conformers of the c-Myc-Max leucine zipper, *Proteins 41*, 485−497.
32. Phelan, P., Gorfe, A. A., Jelesarov, I., Marti, D. N., Warwicker, J., and Bosshard, H. R. (2002) Salt bridges destabilize a leucine zipper designed for maximized ion pairing between helices, *Biochemistry 41*, 2998−3008.
33. Gorfe, A. A., Ferrara, P., Caflisch, A., Marti, D. N., Bosshard, H. R., and Jelesarov, I. (2002) Calculation of protein ionization equilibria with conformational sampling: pK_a of a model leucine zipper, GCN4 and barnase, *Proteins 46*, 41−60.
34. Strop, P., and Mayo, S. L. (2000) Contribution of surface salt bridges to protein stability, *Biochemistry 39*, 1251−1255.
35. Dao-pin, S., Sauer, U., Nicholson, H., and Matthews, B. W. (1991) Contributions of engineered surface salt bridges to the stability of T4 lysozyme determined by directed mutagenesis, *Biochemistry 30*, 7142−7153.
36. Mori, S., Abeygunawardana, C., Johnson, M. O., and Vanzijl, P. C. M. (1995) Improved sensitivity of HSQC spectra of exchanging protons at short interscan delays using a new fast HSQC (FHSQC) detection scheme that avoids water saturation, *J. Magn. Reson., Ser. B 108*, 94−98.
37. Markley, J. L. (1975) Observation of histidine residues in proteins by means of nuclear magnetic resonance spectroscopy, *Acc. Chem. Res. 8*, 70−80.
38. Wüthrich, K., Billeter, M., and Braun, W. (1983) Pseudo-structures for the 20 common amino acids for use in studies of protein conformations by measurements of intramolecular proton−proton distance constraints with nuclear magnetic resonance, *J. Mol. Biol. 169*, 949−961.
39. Brunger, A. T., Adams, P. D., Clore, G. M., DeLano, W. L., Gros, P., Grosse-Kunstleve, R. W., Jiang, J.-S., Kuszewski, J., Nilges, M., Pannu, N. S., Read, R. J., Rice, L. M., Simonson, T., and Warren, G. L. (1998) Crystallography & NMR system: a new software suite for macromolecular structure determination, *Acta Crystallogr. D54*, 905−921.
40. Laskowski, R. A., MacArthur, M. W., Moss, D. S., and Thornton, J. M. (1993) PROCHECK: a program to check the stereochemical quality of protein structures, *J. Appl. Crystallogr. 26*, 283−291.
41. Vriend, G. (1990) WHAT IF: a molecular modeling and drug design program, *J. Mol. Graphics 8*, 52−56.
42. Koradi, R., Billeter, M., and Wuthrich, K. (1996) MOLMOL: a program for display and analysis of macromolecular structures, *J. Mol. Graphics 14*, 51−55.
43. Jorgensen, W. L., Chandrasekhar, J., Madura, J. D., Impey, R. W., and Klein, M. L. (1983) Comparison of simple potential functions for simulating liquid water, *J. Chem. Phys. 79*, 926−935.
44. Brooks, B. R., Bruccoleri, R. E., Olafson, B. D., States, D. J., Swaminathan, S., and Karplus, M. (1983) Charmm: A Program for Macromolecular Energy, Minimization, and Dynamics Calculations, *J. Comput. Chem. 4*, 187−217.
45. Yang, A. S., and Honig, B. (1993) On the pH dependence of protein stability, *J. Mol. Biol. 231*, 459−474.
46. Yang, A. S., Gunner, M. R., Sampogna, R., Sharp, K., and Honig, B. (1993) On the calculation of pK_a's in proteins, *Proteins 15*, 252−265.
47. Nicholls, A., and Honig, B. (1991) A rapid finite difference algorithm, utilizing successive over-relaxation to solve the Poisson−Boltzmann equation, *J. Comput. Chem. 12*, 435−445.
48. Antosiewicz, J., McCammon, J. A., and Gilson, M. K. (1994) Prediction of pH-dependent properties of proteins, *J. Mol. Biol. 238*, 415−436.
49. Beroza, P., Fredkin, D. R., Okamura, M. Y., and Feher, G. (1991) Protonation of interacting residues in a protein by a Monte Carlo method: application to lysozyme and the photosynthetic reaction center of *Rhodobacter sphaeroides*, *Proc. Natl. Acad. Sci. U.S.A. 88*, 5804−5808.
50. Nielsen, J. E., and Vriend, G. (2001) Optimizing the hydrogen-bond network in Poisson−Boltzmann equation-based pK_a calculations, *Proteins 43*, 403−412.
51. Jorgensen, W. L., and Tirado-Rives, J. (1988) The OPLS potential functions for proteins. Energy minimizations for crystals of cyclic peptides and crambin, *J. Am. Chem. Soc. 110*, 1657−1666.
52. Wüthrich, K. (1986) *NMR of Proteins and Nucleic Acids*, John Wiley and Sons, New York.
53. Wishart, D. S., Sykes, B. D., and Richards, F. M. (1991) Relationship between nuclear magnetic resonance chemical shift and protein secondary structure, *J. Mol. Biol. 222*, 311−333.
54. Pardi, A., Billeter, M., and Wuthrich, K. (1984) Calibration of the angular dependence of the amide proton-C α proton coupling constants, $^3J_{HN-\alpha}$, in a globular protein. Use of $^3J_{HN-\alpha}$ for identification of helical secondary structure, *J. Mol. Biol. 180*, 741−751.
55. Nozaki, Y., and Tanford, C. (1967) Examination of titration behavior, *Methods Enzymol. 11*, 715−734.

BI048771T